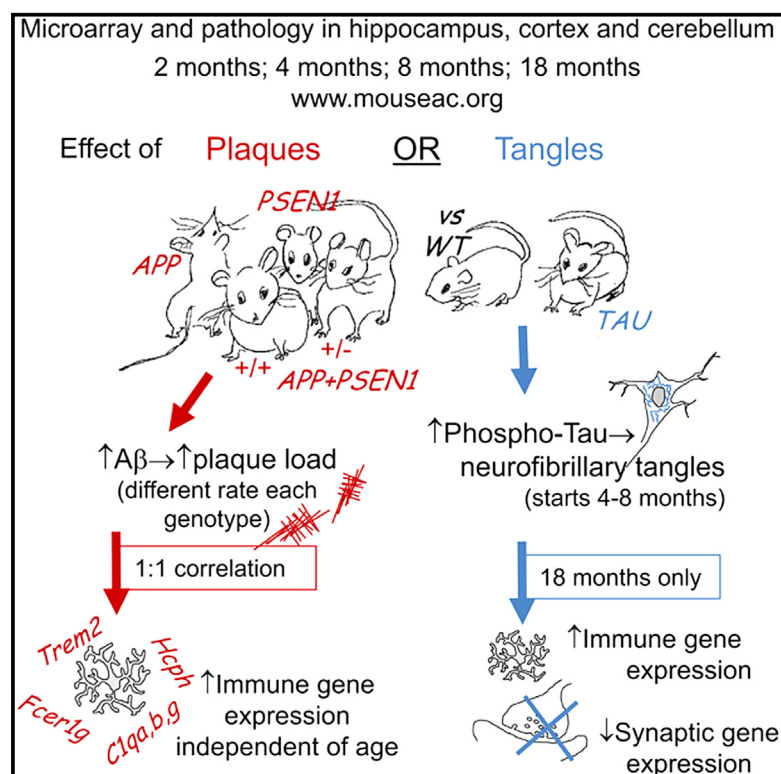


A Genome-wide Gene-Expression Analysis and Database in Transgenic Mice during Development of Amyloid or Tau Pathology

Graphical Abstract



Authors

Mar Matarin, Dervis A. Salih, ...,
John Hardy, Frances A. Edwards

Correspondence

j.hardy@ucl.ac.uk (J.H.),
f.a.edwards@ucl.ac.uk (F.A.E.)

In Brief

In Alzheimer's disease, should we target amyloid and plaques or TAU and tangles? Matarin et al. present a genome-wide gene expression and pathology resource comparing five transgenic mouse lines with only plaques or only tangles, allowing comparison of the separate effects of these pathologies throughout the life of the mouse.

Highlights

- Gene expression in WT and five mouse dementia models; four ages; three brain regions
- Validation of mouse models versus human genome data and network analysis
- In A_β mice, plaques show 1:1 correlation with immune gene expression; all ages
- In old TAU mice, changes in immune and synaptic gene expression correlate with tangles

Accession Numbers

GSE64398

A Genome-wide Gene-Expression Analysis and Database in Transgenic Mice during Development of Amyloid or Tau Pathology

Mar Matarin,^{1,3} Dervis A. Salih,² Marina Yasvoina,² Damian M. Cummings,² Sebastian Guelfi,³ Wenfei Liu,² Muzammil A. Nahaboo Solim,^{2,6} Thomas G. Moens,² Rocio Moreno Paublete,² Shabinah S. Ali,² Marina Perona,¹ Roshni Desai,⁶ Kenneth J. Smith,⁶ Judy Latcham,⁴ Michael Fulleylove,⁴ Jill C. Richardson,⁵ John Hardy,^{3,*} and Frances A. Edwards^{2,*}

¹Department of Clinical and Experimental Epilepsy, Institute of Neurology, Queen Square, London WC1N 3BG, UK

²Department of Neuroscience, Physiology and Pharmacology, UCL, Gower Street, London WC1E 6BT, UK

³Reta Lila Research Laboratories and Department of Molecular Neuroscience, UCL, Institute of Neurology, 1 Wakefield Street, London WC1N 1PJ, UK

⁴Department of Laboratory Animal Science, GlaxoSmithKline R&D, Stevenage SG1 2NY, UK

⁵Neurosciences Therapeutic Area, GlaxoSmithKline R&D, Stevenage SG1 2NY, UK

⁶Department of Neuroinflammation, UCL Institute of Neurology, Queen Square, London WC1N 3BG, UK

*Correspondence: j.hardy@ucl.ac.uk (J.H.), f.a.edwards@ucl.ac.uk (F.A.E.)

<http://dx.doi.org/10.1016/j.celrep.2014.12.041>

This is an open access article under the CC BY license (<http://creativecommons.org/licenses/by/3.0/>).

SUMMARY

We provide microarray data comparing genome-wide differential expression and pathology throughout life in four lines of “amyloid” transgenic mice (mutant human *APP*, *PSEN1*, or *APP/PSEN1*) and “TAU” transgenic mice (mutant human *MAPT* gene). Microarray data were validated by qPCR and by comparison to human studies, including genome-wide association study (GWAS) hits. Immune gene expression correlated tightly with plaques whereas synaptic genes correlated negatively with neurofibrillary tangles. Network analysis of immune gene modules revealed six hub genes in hippocampus of amyloid mice, four in common with cortex. The hippocampal network in TAU mice was similar except that *Trem2* had hub status only in amyloid mice. The cortical network of TAU mice was entirely different with more hub genes and few in common with the other networks, suggesting reasons for specificity of cortical dysfunction in FTDP17. This Resource opens up many areas for investigation. All data are available and searchable at <http://www.mouseac.org>.

INTRODUCTION

During the development of Alzheimer’s disease (AD), changes in gene expression occur at many stages of disease progression. Early changes may be causal, possibly contributing to initial pathology, whereas later changes may be consequential, due to synaptic and neuronal damage. Eventually, amyloid and/or tau deposition and gliosis are thought to result in altered expression of genes including those of the immune system. Although these

latter changes have often been thought of as secondary, and therefore of little note, recent analyses have suggested that genetic variability in immune processes, particularly with respect to microglial responses, is important in determining the risk of individuals presenting with the disease. Although mutations in amyloid precursor protein (APP) or presenilin 1 (PSEN1) or PSEN2 that lead to raised levels of a range of amyloid β (A β) peptides are sufficient to result in Alzheimer’s disease in humans, phosphorylation of microtubule-associated protein tau (tau) and the development of tangles is an essential step in the course of the disease. The relative contribution of these two elements to different aspects of the disease is still a matter of controversy.

With this background, we have embarked on a systematic analysis in which we compare whole-genome expression in five transgenic mice with human genes for dementia that result in either plaques or tangle pathology to the expression in wild-type (WT) control mice and to each other. Microarrays have previously been used to investigate gene expression in a range of different studies and have been extensively verified in mice and humans (Lagraoui et al., 2012; Trabzuni et al., 2011). After quality control steps, excluding probes or mice with insufficient signal (see [Experimental Procedures](#)), data were available for 12,588 genes and pathology in 113 hippocampus samples, 113 cortex samples, and 111 cerebellum samples. In particular, we have compared mice transgenic for mutant gene(s) relevant either to FTDP17: TAU (*MAPT*: P301L; Hutton et al., 1998) or to AD: TAS10, amyloid precursor protein (*APP*: K670N/M671L; Mullan et al., 1992); TPM, presenilin 1 (*PSEN1*: M146V); or TASTPM (*APP* and *PSEN1* [combining the above], heterozygous [HET] or homozygous [HO]; Howlett and Richardson, 2009). This analysis allows comparison of the relation of gene expression to development of neurofibrillary tangles versus development of amyloid plaques and, in the case of the amyloid mice, also allows study of dose dependency, as both total A β and plaque load develop in these mice at different rates.

In all of these mouse lines, we have measured pathology and, in the same mice, gene expression changes at 2, 4, 8, and 18 months in the hippocampus, cortex, and cerebellum, covering the period before and during development of plaques or tangles. In this initial study, we take two approaches. We report an unbiased genome-wide microarray analysis of mRNA, comparing genotypes across all ages and brain regions and investigating networks and nodes that arise when considering all the genes that show differences in expression compared to WT mice. In addition, we describe changes in expression of genes known as risk factors from previous genome-wide association studies (GWASs).

The analysis of data in these different models at ages before and during the development of pathology in hippocampus, cortex, and cerebellum greatly extends previous reports of the increased expression of genes in the immune system as plaques develop in hippocampus or cortex (Dickey et al., 2003; Frautschy et al., 1998; Howlett et al., 2008; Reddy et al., 2004; Stein and Johnson, 2002; Wirz et al., 2013; Wu et al., 2006). We make all the data publicly available at <http://www.mouseac.org>. In addition to access to the full set of data, the database of normalized genes can be searched across age for individual gene expression in WT mice and any combination of the models with both graphical and numerical outputs, thus providing information relevant to normal aging and to both amyloid and TAU models.

RESULTS AND DISCUSSION

Rate and Extent of Development of Amyloid Plaques and Neurofibrillary Tangles in Mice Used for Gene-Expression Studies

As we aimed to identify and compare any expression changes that occur with the development of pathology in the different models, we investigated the level of amyloid plaque burden and phosphorylated tau pathology (hippocampus, Figure 1; cortex, Figure S1). For each mouse, mRNA was extracted from one brain hemisphere and the other hemisphere was used for immunohistochemistry.

In general, the hippocampus and cortex showed similar plaque development. The mouse lines studied showed different time courses of plaque load progression, allowing us to study gene-expression changes related to progression of this pathology. TASTPM (APP/PSEN1) mice showed the strongest phenotype. In agreement with the initial characterization of TASTPM mice (Howlett and Richardson, 2009), HO-TASTPM started to show diffuse amyloid staining at 2 months but developed true plaques by 4 months. In these mice, by 8 months, small plaques are scattered densely throughout the tissue, and by 18 months, much of the hippocampus and cortex are covered in large plaques. The HET-TASTPM mice show a similar pattern but developing more slowly, whereas the TAS10 mice (APP only) also show plaques but only at 18 months. TPM mice (PSEN1 only) show no sign of plaques at any time. In contrast, neurofibrillary tangles are only found in the TAU mice with rare tangles starting to appear in cortex in some mice at 4 months. By 8 months, they are seen in all mice in the hippocampus and cortex, and by 18 months, neurofibrillary tangles are present in almost all neurons in these regions.

No plaques or tangles were found in the cerebellum of any of the mice, consistent with the lack of plaques in this region previously observed in mouse models (Manook et al., 2012) and the very mild plaque load observed even at end stage in live imaging or postmortem tissue from AD patients (Driscoll et al., 2012; Thal et al., 2004).

Microarray Data

Little Change in the Endogenous Expression of Mouse App, Psen1, or Mapt

We initially checked whether overexpression of human genes had caused any compensatory effects on the equivalent mouse genes. We found no evidence that mouse *App*, *Psen1*, or *Mapt* were changed in expression in any of the APP or PSEN1 transgenic mice (Figure S3; Table S1). In TAU mice, expression levels of mouse *App* and *Mapt* were slightly reduced. This is an important observation, as it means there is no evidence that expression of the human transgenes causes increases in expression of any of these directly related mouse genes in a manner that could result in a feed-forward loop for amyloid pathogenesis. (As *Psen1* was not detectable on the microarray, its expression was tested with qPCR; Figure S3).

Genome-wide Expression Analysis

Differential gene expression is correlated with pathology in the different lines of amyloid mice, with TAU mice showing later changes but reaching similar numbers of differentially expressed genes.

Initially, differential gene expression was examined across all ages and all genotypes, particularly concentrating on large changes in expression compared to WT mice (at least 2-fold; false discovery rate [FDR] ≤ 0.05). In all the amyloid lines (HO- and HET-TASTPM, TAS10 [APP], and TPM [PSEN1]), the pattern of gene expression was similar to the pattern of the pathology described above (Table S2). As with pathology, the largest and earliest effects in gene expression were in the double mutants, particularly HO-TASTPM with the HET-TASTPM showing a qualitatively similar pattern of change, albeit at a slightly lower level throughout. Interestingly, when the two mutations were expressed separately in the TAS10 (APP) or TPM (PSEN1) mice, very little change in gene expression was seen, again consistent with the extent of pathology and confirming that the large progressive gene-expression changes are not primarily age related. The exception in the single transgenics was a small number of genes that were differentially expressed in the TPM mice at the earliest age tested (2 months; Table S2). These included genes related to brain development (*Msx1*, *Otx2*, and *Zic4*), consistent with the known role of *PSEN1* in development through its role in Notch processing (Hartmann et al., 1999). This suggests that these mice may have a slightly retarded hippocampal-development profile.

As the expression changes seen in the different amyloid mice showed a similar pattern except that they occurred at rates related to the rate of plaque deposition and hence at different ages, we will include all genotypes in the network analysis below but otherwise restrict the description in this paper to the HO-TASTPM mice, representing the most clearly measureable changes. Other details are included in the supplemental tables referred to throughout the text. In contrast in TAU mice, whereas

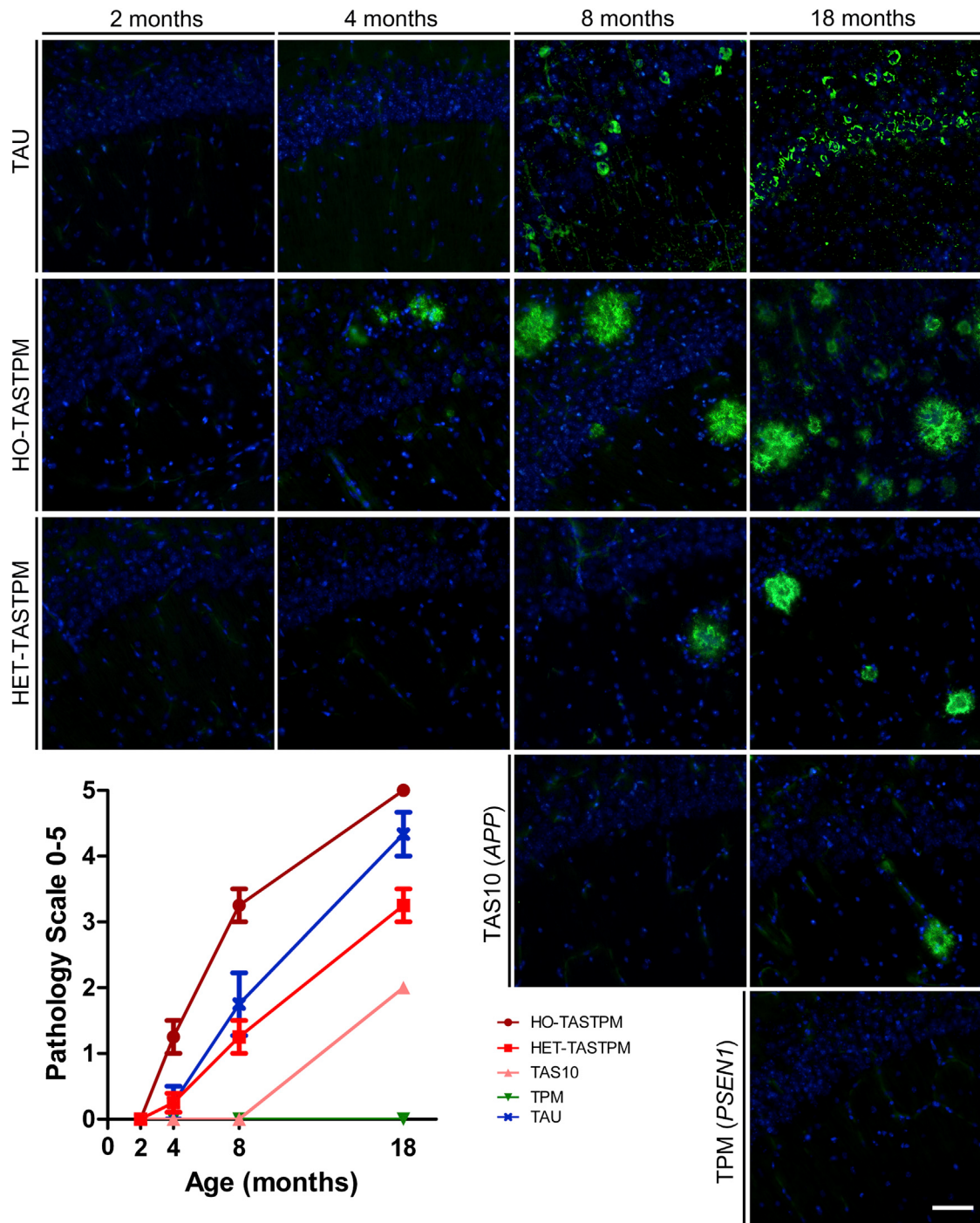


Figure 1. Development of Pathology in the Hippocampus of TAU, TASTPM, TAS10, and TPM Transgenic Mice

Representative images of the CA1 region in the hippocampus, immunostained with antibodies (green) for A β -40 or phosphorylated tau (AT8) and nuclear stain DAPI (blue). TAU mice show phosphorylated tau in neurons and dendrites, usually beginning at 8 months of age. At 18 months, the majority of neurons in the cell layers contain phosphorylated tau in the cell body. HO-TASTPM mice show early and rapid development of amyloid plaques. HET-TASTPM show slower development of mature plaques beginning at 8 months of age. (Rare small plaques seen at 4 months in most mice.) TAS10 (APP) mice develop sparse hippocampal plaques by 18 months of age. TPM (PSEN1) mice show no evidence of amyloid deposition by 18 months. Error bars: SEM. The scale bar represents 50 μ m. See Figure S1 for progression of pathology in the cortex, which is similar to hippocampus in all groups.

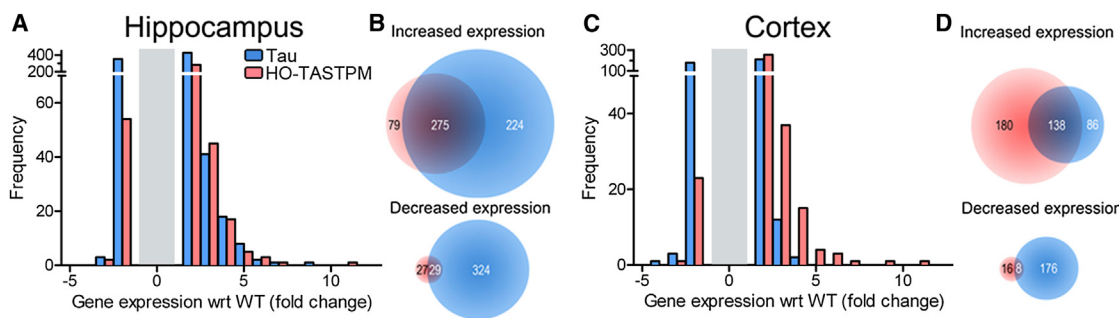


Figure 2. Frequency of Gene Expression Changes Compared to WT, FDR < 0.05, Occurring in HO-TASTPM and/or TAU Mice at 18 Months of Age in Hippocampus and Cortex

(A and B) Hippocampus.

(C and D) Cortex.

(A and C) x axes represent fold changes (increased expression, positive; decreased expression, negative; negative fold change defined as $-1/(transgenic/WT)$ expression); gray area undefined [1 or -1 , no change]; HO-TASTPM [red] and TAU [blue]; Y axes represent frequency of genes).

(B and D) Venn diagrams depicting the overlap between genes with increased or decreased expression in TAU and HO-TASTPM (>1.5 -fold changes).

See Tables S2–S4 for numbers of genes for these and other genotypes and details of genes differentially expressed.

the number of genes showing differential expression at 18 months was similar to HO-TASTPM, the changes occurred considerably later, lagging several months behind the appearance of neurofibrillary tangles, with relatively little change in gene expression seen at earlier stages. Whereas hippocampal and cortical patterns of expression were similar, although with fewer genes affected in the cortex, very few genes were differentially expressed in the cerebellum in any genotype, as expected. The descriptions below thus relate to hippocampus unless otherwise specified.

General Patterns of Changes 2–18 Months: Heterogeneous Pattern of Early Gene Expression in Hippocampus

In HO-TASTPM mice, a few genes involved in neuronal differentiation or development showed differential increases in expression (e.g., *Dlx1*, *Efna5*, and *Gap43*) at 2 months of age before true amyloid plaques developed (Table S4). By 4 months, genes in these developmental categories showed a mixture of increased and decreased expression when compared with WT mice but stabilized to WT levels by 8 months.

A similar pattern was seen in synapse-related genes in HO-TASTPM. At 4 months, 20 of these genes showed increased expression compared to WT, whereas ten other genes within this category showed lower expression together with significantly decreased expression of 15 genes involved in calcium signaling. These expression changes returned to WT levels with age and the development of pathology, showing lower expression in a few genes at 8 months. However, in HO-TASTPM at 18 months, synaptic gene expression was almost entirely at WT levels (Tables S1 and S4).

In the TAU mice, the early pattern of expression changes for synaptic genes was similar, showing a mixed picture of a few genes increased and some decreased at 4 months as compared to WT (Tables S2 and S4).

Again genes involved in the calcium signaling pathway showed lower expression, whereas genes involved in cation channel activity or regulation of neurogenesis were increased in expression. These changes were again reversed at 8 months. However, by

18 months, when neurofibrillary tangles were present in almost all neurons, a substantial decrease of expression of synaptic genes was evident, consistent with a loss of synapses.

Hence, whereas early expression changes in synaptic genes were similarly mixed at young ages in amyloid and TAU mice, the loss of synaptic genes at later stages, likely related to loss of synapses, was much more prominent in the TAU mice with little change in amyloid mice.

In fact, in general, very few genes were decreased in expression in HO-TASTPM mice even at 18 months when the plaque load was very heavy. When genes showing increased and decreased expression (>2 -fold; FDR < 0.05) were compared separately at 18 months, we found that, in HO-TASTPM mice, over 97% of the genes that showed differential expression were increased compared to WT in both hippocampus and cortex, with $<3\%$ showing decreased expression. In contrast, in the TAU mice, 15% of differentially expressed genes in hippocampus and 54% in cortex showed significantly lower expression than in WT mice (Table S3).

Genes Common to HO-TASTPM and TAU Mice at 18 Months Are Involved in the Immune System

We went on to investigate whether there was an overlap between these strongly differentially expressed genes in the oldest TAU and the oldest HO-TASTPM mice and characterized the function of such common genes using the Enrichment Analysis Systematic Explorer (EASE) in DAVID (<http://david.abcc.ncifcrf.gov>; Table S4).

At 18 months, a striking number of genes showed increased expression (<2 -fold) compared to WT mice in both the HO-TASTPM and TAU mice, particularly in the hippocampus with 106 genes (52%) in common from a total of 202 overexpressed genes and a similar proportion (48%) when the threshold was lowered to 1.5-fold (Figures 2A and 2B; Table S3). The overlapping genes were largely related to immune or inflammatory responses, in both the hippocampus and cortex (Table S4). In the HO-TASTPM mice, even those genes not common to the TAU mice tended to fall into the immune response category. In contrast, in TAU mice, nonoverlapping genes tended to be

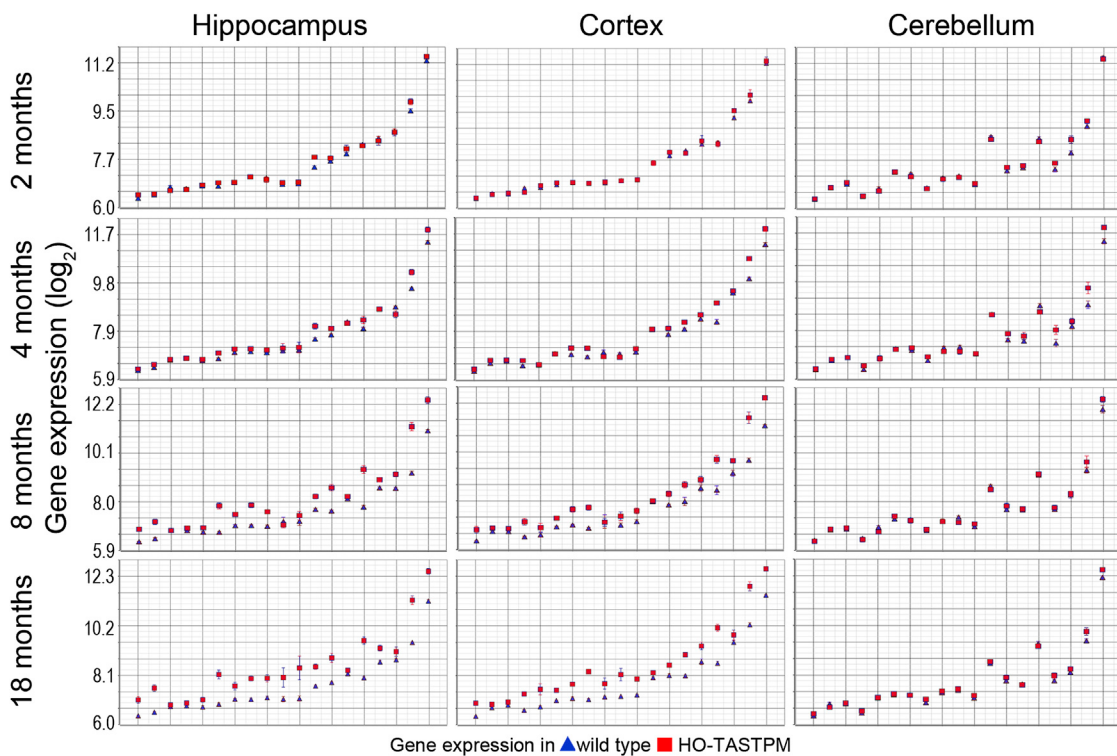


Figure 3. Complete Disruption of the Gene Ontology Category “Antigen Processing and Protein Presentation” in HO-TASTPM

Each symbol corresponds to the expression of an individual gene (HO-TASTPM, red squares; WT, blue triangles). Progressive disruption of this functional category starts at 4 months and with complete disruption by 18 months in both hippocampus and cortex. Hippocampus shows the largest expression changes, followed by the cortex, with almost no change in the cerebellum. See Table S4 for completely disrupted Gene Ontology (GO) categories in HO-TASTPM and TAU mice.

involved in cell death or apoptosis (12 genes) and DNA packaging or chromatin assembly and disassembly (12 genes; Table S4), again suggesting that loss of neurones or synapses was likely more prominent in these mice.

HO-TASTPM and TAU Mice Show Changes in Entire GO Categories Involved in Immune Function

Gene Ontology (GO)-ANOVA analysis of complete functional groupings of genes (by averaging member gene expression of GO categories with a minimum of 15 and maximum of 300 genes) also confirmed considerable disruption in the immune system. Eighteen entire GO categories were differentially increased in hippocampus of HO-TASTPM mice, and of these, eight were also increased in cortex. Moreover, even at 8 months, eight categories were increased in hippocampus and two in cortex. These GO categories were again related to the immune response. At 4 months, two other GO categories related to hormone activity and regulation were also increased in the hippocampus of HO-TASTPM mice. The general pattern of disruption confirmed the observations above of increasing disruption in parallel with amyloid pathology in both hippocampus and to a lesser extent cortex, but little if any disruption in cerebellum (for example see Figure 3).

Nineteen GO categories were found to be altered in the TAU mice at 18 months in the hippocampus and in the cortex; GO categories increasing in TAU mice were all also increased in

the HO-TASTPM (Table S4). No GO category was found dysregulated at other ages or in the cerebellum at any age.

Analysis of Genes Defined as Risk Factors by Alzheimer’s GWASs Show Dysregulation in Both TASTPM and TAU Mice

Although our primary analysis was genome-wide, we were particularly interested in investigating the effects on gene expression for all the known risk genes for AD in order to dissect how the development of pathology influences their expression (Figure 4, see legend for list of genes tested; Table S1). Although the fact that a variant of a particular gene represents a risk factor does not automatically imply that the normal sequence cognate protein will be directly involved in the pathogenesis of the disease, some of these genes would be likely to show expression changes during disease progression. This will give additional evidence of the identification of the risk genes, as one of the weaknesses of GWASs comes from the fact that the variants or loci identified can be some distance from the protein-coding sequences of any gene, making the link to the gene uncertain (Guerreiro and Hardy, 2011). Changes in these genes would both contribute evidence to the validity of the models but also add to the knowledge of their role in disease progression. Interestingly, at 18 months in hippocampus, expression of the following GWAS loci risk genes was differentially increased by at least 1.5-fold in both the HO-TASTPM and TAU

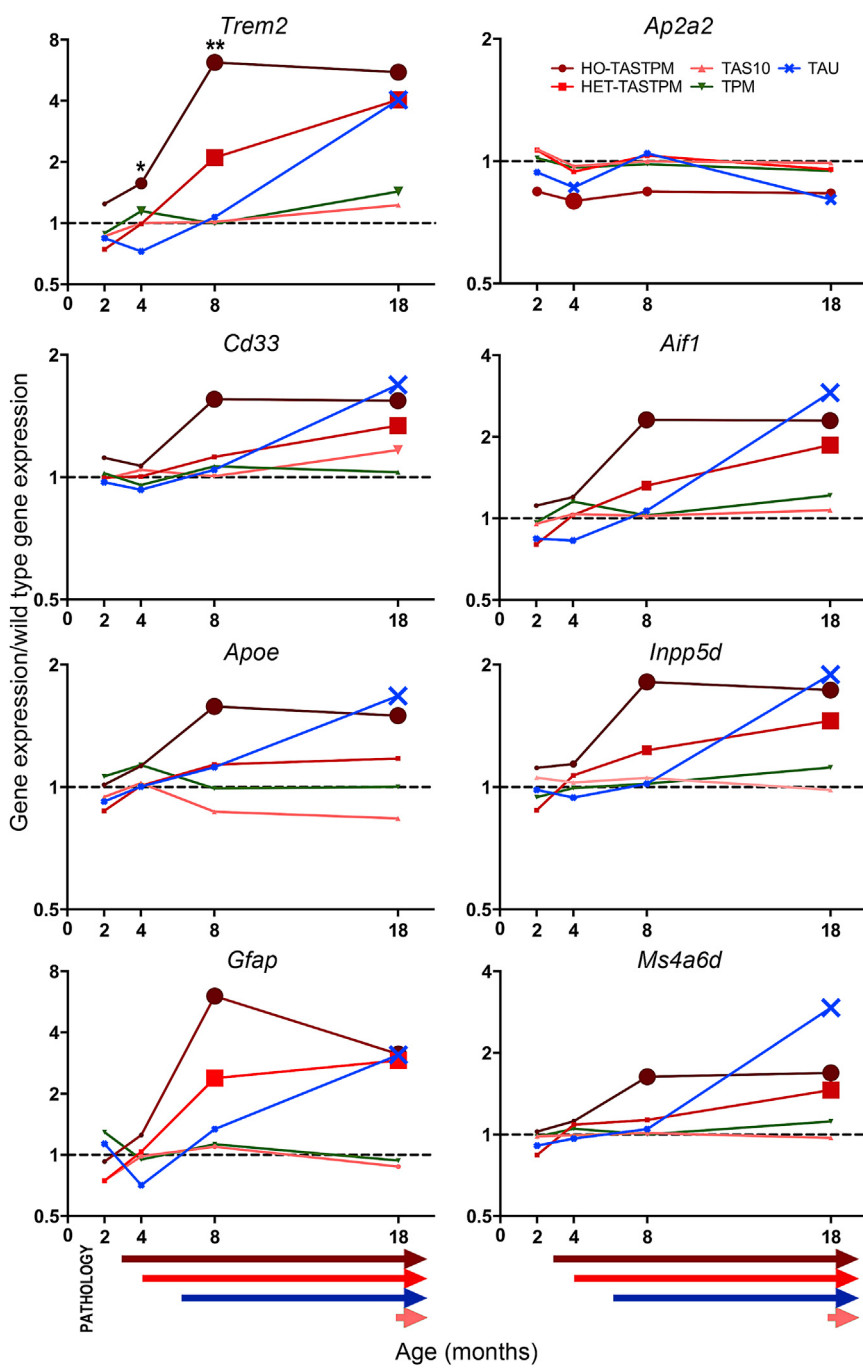


Figure 4. Gene Expression Changes Relative to WT of Risk Factor or Other AD-Related Genes

Largest symbols $p < 0.0001$ (** on *Trem2* plot); medium $p < 0.01$ (*) on *Trem2* plot). Small symbols, no significant difference. For graphical representation here, errors are excluded, but individual gene data are available at <http://mouseac.org>. Arrows at the bottom indicate the time course from appearance of plaques or neurofibrillary tangles. Legend indicating colors of symbols and arrows top right applies to all panels. Genes tested: *Abca7*; *Ace*; *Aif1*; *Ap2a2*; *Apoe*; *App*; *Bin1*; *Cd33*; *Clu*; *Cugbp1*; *Dsg2*; *Echdc3*; *Frmd6*; *Gfap* (astrocyte marker); *Gria2* (neuron marker); *Hs3st1*; *Inpp5d*; *Mapt*; *Mef2c*; *Mog* (oligodendrocyte biomarker); *Ms4a6d*; *Picalm*; *Psen2*; *Ptk2b*; *Rin3*; *Sic24a4*; *Sorl1*; *Sqstm1*; *Trem2*; *Trip4*; and *Zcwpw1* (genes underlined include >1.5 -fold and FDR $p < 0.05$ for at least one age). See Table S1 for expression of other GWAS hits and Figure S3 for *Psen1* expression by qPCR.

allows the appearance of tangles but with some delay. Similar results were seen for TAU mice in the other genes, with very few genes following the time course of the appearance of neurofibrillary tangles but many showing differential expression at 18 months. Among the immune genes, increased expression of the general microglial marker *Iba1* (*Aif1*) suggests proliferation of microglia numbers. This began from early ages in TASTPM mice but was not detectable until 18 months in TAU mice. This difference was confirmed by qPCR in both the same mice and independent mice (Figure 5A for *Aif1* and Figure S2 for this and other genes) as well as by immunohistochemistry for verification at the protein level (Figures 5B and 5C). However, the even greater increases in *Trem2* suggest additionally a change in activation state of the microglia with individual microglia increasing their *Trem2* expression, as suggested in a previous study comparing plaque-associated and plaque-free tissue in which TREM2 was

mice: *Apoe*; *Cd33*; *Inpp5d*; *Ms4a6d*; and *Trem2*. Of these, *Trem2* in HO-TASTPM mice showed the greatest differential expression, reaching >5 -fold WT levels by 18 months in both hippocampus and cortex. Expression of all of these genes was however already increased in hippocampus of HO-TASTPM mice from 8 months and, in the case of *Trem2*, from 4 months onward in both cortex and hippocampus. In contrast, in the TAU mice at 8 months, despite neurofibrillary tangles appearing in all mice, no changes in *Trem2* expression were evident, suggesting that the increase in *Trem2* expression fol-

increased but numbers of microglia were unchanged in an amyloid transgenic mouse line (Frank et al., 2008). This is also reflected in the stronger signal for CD68 (Figure 5D). Additionally, two other known risk genes, *Ptk2b* and *Sic24a4*, were significantly decreased by at least 33% in TAU mice at 18 months, but not in HO-TASTPM, and *Ap2a2* was slightly but significantly decreased at 4 months in both TAU and HO-TASTPM (Figure 4). Hence, it seems that at least some of the genes known to be risk factors are indeed directly involved in the effects of increasing A β and/or altered tau function.

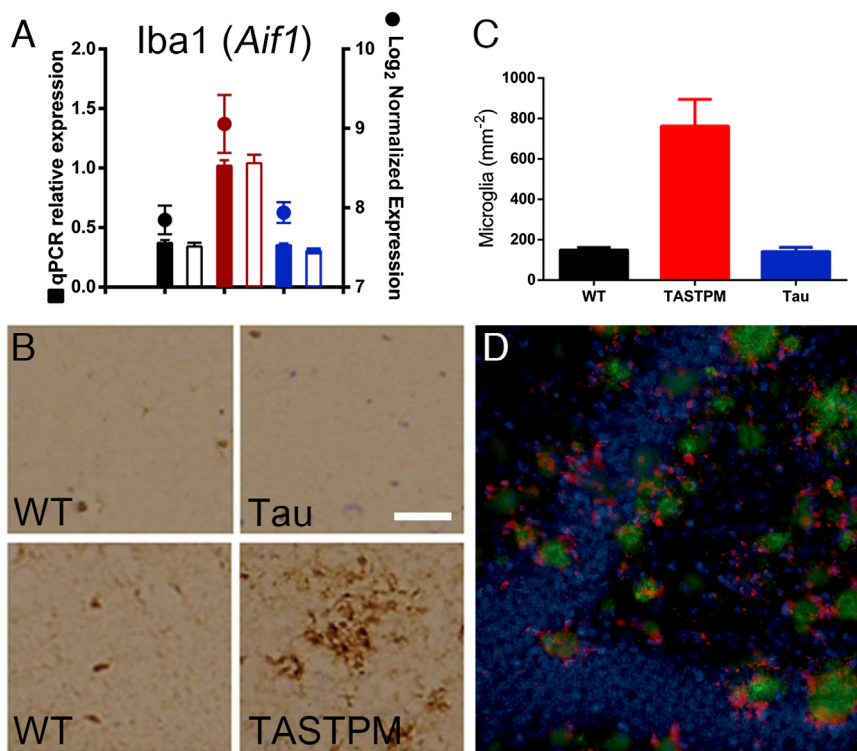


Figure 5. qPCR and Immunohistochemistry Validate the Microarray Data and the Correlation of Plaques Rather Than Tangles to Immune Genes

(A) Iba expression from microarray data (points) is reflected closely by qPCR analysis of mRNA in the same mice (closed bars) and in independent mice (open bars; black, WT; red, HO-TASTPM; blue, Tau). Eight months of age. Error bars: SEM.

(B) Light micrographs of DAB-immunostained brain sections for Iba1 to label microglia in the CA3 region of the hippocampus in Tau or HET-TASTPM mice at 10 months of age. WT and transgenic sample pairs stained simultaneously on the same slide.

(C) Quantification of microglial counts; WT: n = 8 animals; TASTPM: n = 3; Tau: n = 5 (mean of three sections per animal). As WT counts for the two groups were not different, they were combined in this graph. One-way ANOVA, post hoc analysis TASTPM different from WT ($p < 0.0001$). Note that microglia in HO-TASTPM mice were too dense to count, and thus heterozygotes were used for this experiment. Error bars: SEM.

(D) Triple-fluorescent immunofluorescent staining confirming that the clustering of microglia was around plaques in the TASTPM mice. Red, CD68; green, Aβ42; blue, DAPI.

The scale bar in (B) represents 50 μm, and the same scale bar represents 40 μm in (D). (See further qPCR validation of this and other genes in Figure S2 and qPCR of PSEN1 in Figure S3.)

Consistent with changes seen across neurodegenerative diseases in humans, astrocyte marker *Gfap* was also increased from 8 months onward in TAU and TASTPM mice (Figure 4).

Network Analysis of Differentially Expressed Genes in the Transgenic Mice

Weighted Gene Co-expression Network Analysis (WGCNA) was applied to genes with high variable expression with the following aims: (1) to identify novel gene coexpression modules and summarize the main enriched biological functions and molecular pathways that are disrupted in the AD transgenic models and (2) to investigate whether expression levels of confirmed and proposed AD loci belong to specific modules and to understand which genes they correlated with in putative disease pathways. (See the *Experimental Procedures* for further details).

Unsupervised WGCNAs were used to analyze the most-variable genes (n = 3,904) determined by their coefficient of variance and not in relation to clinical or pathological features.

Separate coexpression networks for the transgenic and WT groups confirmed that nearly all of the networks of WT mice were preserved in the transgenic mice. Overall, we found strong evidence of preservation of the WT modules (Z summary > 10) in the transgenic modules in the three brain regions, indicating similar basic transcriptional organization in the brain.

To investigate how groups of coexpressed genes showing transcriptional differences between transgenic and WT mice were related to the occurrence of amyloid plaques or neurofibrillary tangles, we constructed a coexpression network using samples from all transgenic and WT mice throughout the

ages tested. The expression levels of each module were summarized by the first principal component and related to variables such as age (2, 4, 8, and 18 months), amyloid or tau pathology, genotype (all transgenic versus WT mice), individual transgenic lines, and interactions between these variables. In addition, potential artifacts due to technical experiment variables, such as hybridization batch, were tested, though they were not determined to be statistically significant, and therefore excluded.

In the hippocampus, two significant modules of coexpressed genes were identified: M1 ($r^2 = 0.43$; $p = 3 \times 10^{-6}$), a module enriched with genes associated with immune and inflammatory processes and M2 ($r^2 = -0.5$; $p = 2 \times 10^{-8}$), a module enriched with genes involved in synapse and neurotransmitter transport functions (Figure 6A; Table S5 for GO categories in M1 and M2).

The immune module, M1, was correlated with genetic modification ($r^2 = 0.26$; $p = 0.005$), age ($r^2 = 0.48$; $p = 7 \times 10^{-8}$), mouse line ($r^2 = 0.38$; $p = 4 \times 10^{-5}$), and also with the interaction between age and genetic modification ($r^2 = 0.57$; $p = 3 \times 10^{-11}$) and age and mouse line ($r^2 = 0.54$; $p = 7 \times 10^{-10}$) but was most strongly positively correlated with amyloid pathology and less strongly but still showing high statistical significance with tau pathology (Figure 6Aii). Of all these relationships, the strongest correlation was between the immune module M1 and amyloid pathology in the general analysis of genes from all mice. We went on to investigate this correlation, removing the TAU mice from this comparison, as they had a transgenic alteration not related to plaque pathology. Including only amyloid and WT

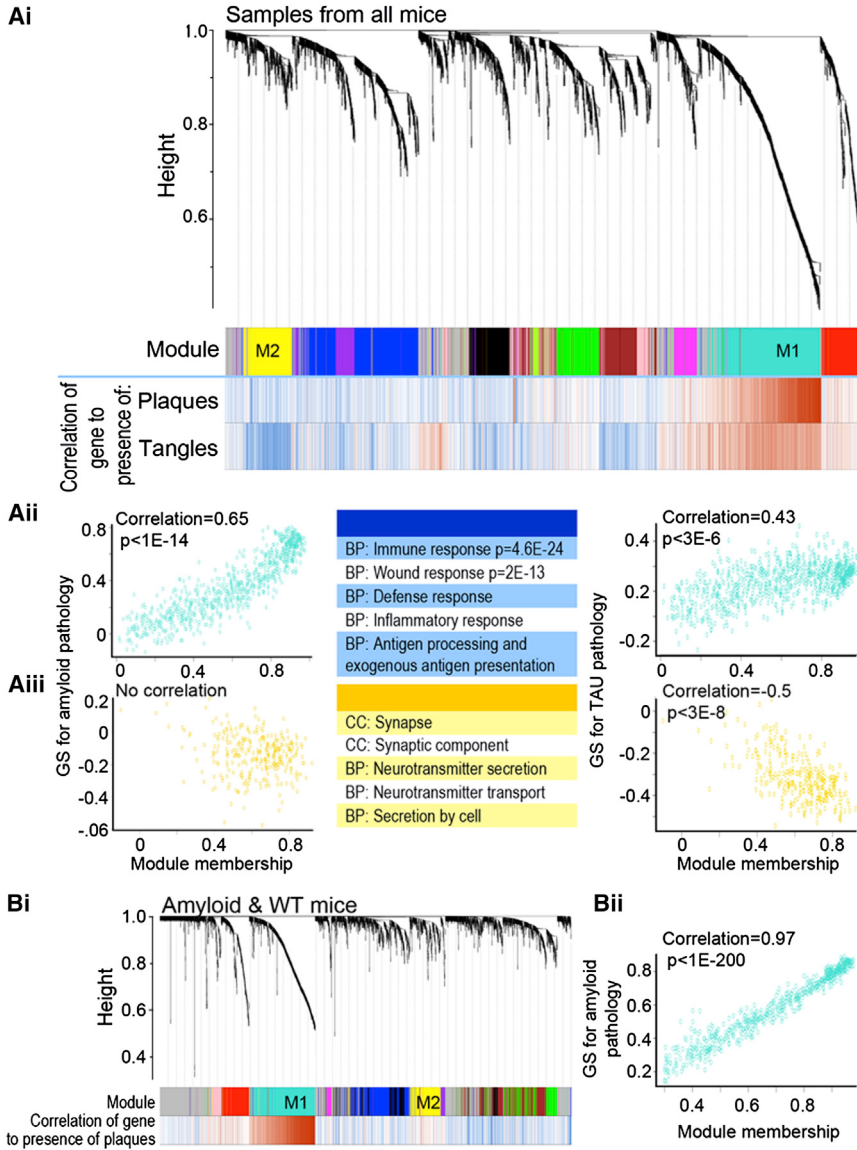


Figure 6. Analysis of Gene Coexpression and the Relation of Significant Modules to Amyloid or Tau Pathology

(A) Network analysis of the most-correlated genes across all genotypes and ages. (i) Dendrogram of average hierarchical gene clustering (modules are divided at significant branch points in the dendrogram). The y axis corresponds to the distance determined by the extent of topological overlap. The first band below the x axis shows the resulting automatically determined modules only referring to correlation of gene expression without biological considerations. The lower two bands illustrates a measure of biological relevance (“gene significance” [GS]) of the modules in terms of positive (red) or negative (blue) correlation of participating genes to amyloid or tau pathology. (ii) Module membership (measure of the correlation between the gene-expression profile and the module’s gene-expression profile) for genes from all mice, as indicated in (i) plotted against GS. M1 (“immune module”) membership correlation with amyloid (left) and tau (right) pathology. (iii) M2 (“synapse module”) membership correlation with amyloid (left) or tau (right) pathology. The central panels in both (ii) and (iii) list the functions of the genes most strongly represented in the modules illustrated, with the strongest correlation being M1 to amyloid pathology. BP and CC indicate whether the modules are according to biological processes or cellular compartments.

(B) As for (A) above, but only analyzing genes of amyloid mice and WT. Note the very strong correlation of M1 to plaque load when analysis is restricted to amyloid mouse lines. (See Table S5 for details of GO categories for M1 and M2.)

mice again brought out M1 as the strongest module and strongly increased the correlation of M1 and amyloid pathology to a level close to 1:1 (Figure 6B). Similar strong correlations were found in the cortex. Again, whereas it is not unexpected that changes in immune function may be a reaction to plaque deposition, the strength of this correlation was unexpected. Hence, it seems that amyloid pathology alone is sufficient to activate the immune system and the role of tau pathology in this context is considerably weaker. The earlier increases in immune function in TASTPM mice compared to TAU mice were confirmed with immunohistochemistry as outlined above (Figure 5). The microglia were seen especially, but not entirely, to cluster around plaques (Figure 5D).

In contrast, the synaptic module M2, whereas also correlating with age ($r^2 = -0.27$; $p = 0.005$) and the interaction between age and genetic modification ($r^2 = -0.37$; $p = 6 \times 10^{-5}$) and mouse line ($r^2 = -0.33$; $p = 3 \times 10^{-4}$), correlated negatively with tau pa-

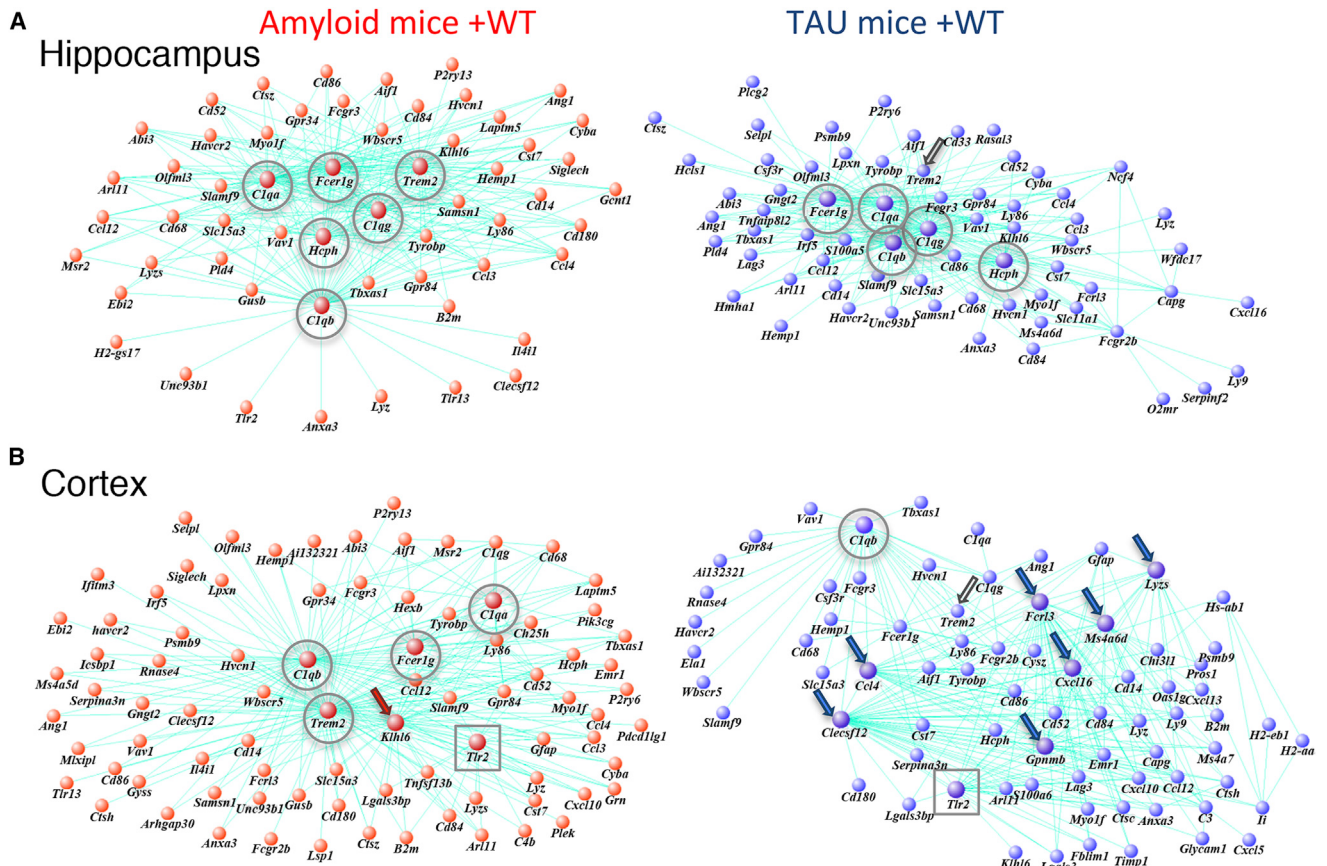
thology but showed no significant correlation with amyloid pathology (adjusted p value > 0.01 ; Figure 6Aiii). The negative correlation of synaptic genes to tau pathology is consistent with postmortem tissues from Alzheimer’s patients, where synaptic loss has been shown to be

correlated with the presence of tau tangles in cortical pyramidal neurons (Merino-Serrais et al., 2013).

Immune Module, AD Risk Loci, and Connectivity Patterns

The immune module M1 was particularly of interest because it included several of the human risk factors for AD, as defined by GWASs. As expected, *Trem2* and *Cd33*, as well as *Inpp5d* and *Ms4a6d*, were included. Having established the strong correlation between gene significance (GS) and module membership when all the amyloid mouse lines (HO- and HET-TASTPM, TAS10, and TPM) and WT mice were considered together, we went on to investigate which of the genes in this module were of particular importance in terms of interconnectivity in the network (Figure 7).

In a complex network, connectivity frequently follows a power law distribution in which only a few nodes show very high

**Figure 7. Network Analysis of Immune Genes**

Network plot using VisANT reveals key drivers of the “immune” module (M1) using genes from either WT and amyloid mice (left) or WT and TAU mice (right). Genes are connected to all other genes that show significant correlation of gene expression. Larger spheres represent “hub genes,” those showing the greatest number of connections to other genes in the network.

(A) Hippocampus. The only difference in genes with hub status between amyloid and TAU mice in hippocampus is *Trem2*, which is a hub gene in the amyloid mice, but not in the TAU mice.

(B) Cortex. The amyloid mice show fewer hub genes than in hippocampus, but all except two of the hubs are in common with hippocampus whereas TAU mice show a different group of hub genes. Circles and squares represent hub genes preserved between brain regions and/or genotypes. Red and blue arrows indicate hub genes not having hub status in any other network plot. Open black arrow in right panels highlights nonhub *Trem2*.

connectivity (Barabási and Oltvai, 2004). There is evidence to suggest that genes with high connectivity (“hub genes,” defined here as genes with at least 15 connections) are crucial to the integrity and proper functioning of the network, making them excellent candidate genes for disease-association studies (Varki et al., 2008). In order to compare the functional network in hippocampus and cortex, and to establish whether amyloid and TAU mice were fundamentally different in the underlying pathways, four networks of genes were constructed dependent on their correlated expression, using genes from the M1 “immune” module either from WT + amyloid mice or WT + TAU mice in both hippocampus and cortex.

Considering only the gene expression in the M1 immune module in the hippocampus of the amyloid + WT mice, the network identified was remarkably simple, centering around only six hub genes (*C1qa*, *C1qb*, *C1qg*, *Fcer1g*, *Hcph*, and *Trem2*; Figure 7A, left panel). Note that *C1qa*, *C1qb*, and *C1qg* code for the three chains of C1q, one of the proteins

that make up the C1 complex, activation of which triggers the classical pathway of the immune complement system (Ghai et al., 2007), bringing the number of hub genes effectively down to only four. In the cortex, a similar pattern was seen as in the hippocampus for the amyloid mice but with only five hub genes (*C1qa*, *C1qb*, *Fcer1g*, *Trem2*, and *Tlr2*), of which all except *Tlr2* are in common with the hippocampal network of these mice. In the hippocampus, the TAU + WT mice also showed almost identical hub genes with the exception of *Trem2*, which, although still part of the correlated network, lost its hub status. This is interesting in terms of the fact that variations in *TREM2* have recently been described as relatively strong risk factors for developing Alzheimer’s disease (Guerreiro et al., 2013; Jonsson et al., 2013) and here appear as particularly important in the network of the amyloid rather than the TAU mice. Considering these hub genes arise from over 600 genes in the immune module M1, the consistency in these three networks is remarkable.

In contrast to the other three networks, in the cortex of the TAU mice, the genes of the M1 module form a more complex network of correlations with ten hub genes, only two of which (*C1qb* and *Tlr2*) are in common with nine hubs of any of the other networks. Hence, *C1qb* is the only gene common to all four networks whereas *Tlr2* is specific to the two cortical networks. The remarkable difference between the cortical network of the TAU mice compared to other three very similar networks is interesting and may suggest reasons why FTD-17 is primarily a cortical disease and shows very different characteristics to AD (Hutton et al., 1998).

Conclusions

We have presented a database that not only goes further than previous such studies in the number of models, ages, and brain regions compared, but we also directly compare transgenic mice with raised A β and plaque pathology but no neurofibrillary tangles to those with a tau mutation leading to tangle pathology without plaques. Network analysis of this extensive database not only validates the models in terms of the relevance of the mouse gene expression to what is known of human genetics in Alzheimer's disease but provides substantial insights into the different effects of alterations in A β and tau. In addition, we highlight specific genes, particularly in the immune system, that may influence the progression of the disease and reveal some of the early synaptic changes that may be important in the onset of disease versus the late synaptic changes that are probably the result of synaptic loss. The separation of the influence of amyloid pathology on immune function and tau pathology on synaptic loss suggests that targeting the development of tau pathology will be the most effective in slowing cognitive decline late in the disease, whereas targeting plaque pathology would decrease the activation of the immune system.

Not only are insights available from approaches such as those outlined above, but every gene can be individually accessed using the interface provided. Access to this interface and to the data providing information on gene expression for studies of different aspects of dementia throughout pathology development as well as normal aging of the hippocampus, cortex, and cerebellum is available at <http://www.mouseac.org>.

EXPERIMENTAL PROCEDURES

Mice

All procedures were performed in agreement with the UK Animals (Scientific Procedures) Act, 1986, with local ethical agreement and following the GlaxoSmithKline (GSK) statement on the use of animals. Mice of different genotypes were killed by isoflurane overdose followed by cervical dislocation at 2, 4, 8, or 18 months, and one half of the hippocampus, cortex, and cerebellum were dissected out and snap frozen for extraction of mRNA. The other half of the brain was drop fixed in 4% paraformaldehyde for direct comparisons using immunohistochemistry. Tissues from at least three male mice from each of the following five transgenic lines, plus at least eight littermate controls from the original parental lines, were collected. The five mouse lines analyzed were as follows.

TAS10: human APP (K670N/M671L); heterozygous on *Thy1* promoter (Richardson et al., 2003)

TPM: human *PSEN1* (M146V); heterozygous on *Thy1* promoter

HET-TASTPM: heterozygous crosses for both of the APP and *PSEN1* transgenic lines

HO-TASTPM: as above but both transgenes bred to homozygosity
 TAU: human microtubule-associated protein tau (*MAPT*) mutant P301L, heterozygous on *CaMKII* promoter
 WT: age-matched WT mice of the same C57Bl/6j background

Histology

Mouse brains were drop fixed in 4% paraformaldehyde and cryoprotected in 30% sucrose. For fluorescent immunostaining, brains were sectioned using a Leica frozen microtome. Serial 30 μ m thick sections (~360 μ m apart), cut transverse to the hippocampus, were pretreated with 1% Chicago Sky blue to reduce background and elastin fluorescence and processed for immunohistochemistry. Sections were permeabilized in 0.3% Triton-X, blocked in 8% horse serum, and incubated with appropriate primary antibodies overnight. Amyloid plaques were examined using rabbit polyclonal A β 40, which recognizes amino acids 34–40 in human A β protein (1:300; Invitrogen), followed by Alexa-488-conjugated secondary antibody (1:500; Abcam). Hyperphosphorylated tau was stained with mouse monoclonal biotinylated AT8, which recognizes the Ser202/Thr205 phosphorylation site of human tau (1:300; Thermo Scientific) and Alexa-488-conjugated streptavidin (1:500; Molecular Probes). Microglia were stained with rat anti-CD68 antibody (Abd Serotec; 1:500), followed by donkey anti-rat (1:1,000; Jackson Laboratories) secondary. Cell nuclei were stained with DAPI (1:10,000; Sigma). Sections from WT mice immunostained with primary and secondary antibodies were included in each experiment, in addition to sections from 18 months transgenic brains stained with appropriate secondary antibody only. Images were obtained using an EVOS Auto FL microscope (Fisher Scientific). Semiquantitative analysis was performed by visually inspecting at least four serial sections of the brains of each animal. Slides were randomized so that the assessor was blind to the age of the mouse.

Glial immunostaining was performed on 10 μ m thick cryosections (Leica CM1950). Sections were pretreated with hydrogen peroxide and 0.1 M sodium citrate prior to incubation with rabbit anti-Iba1 (1:500; Wako) and processed with peroxidase VECTASTAIN ABC kit and 3,3'-diaminobenzidine (DAB) substrate kit per manufacturer's instructions (Vector Laboratories). Imaging was performed on Zeiss Axiohot microscope (Carl Zeiss). For quantification, three 40,000 μ m 2 regions were selected in the CA3 region of the hippocampus and microglia were quantified using ImageJ (NIH) software.

RNA Extraction and Microarrays

Total RNA from the hippocampus was isolated using the RNeasy Mini Kit (QIAGEN). The quality and concentration of the total RNA was determined using a NanoDrop Spectrophotometer (A260:A280 and A260:A230 ratios). All samples (transgenic and WT) were randomly hybridized to Illumina Ref8 v2 microarrays. cDNA labeling and hybridization were performed according to the manufacturer's instructions by AROS Applied Biotechnology.

Verification of Microarray Data with qPCR

As an addition to verification of previous microarray data (Lagraoui et al., 2012; Trabzuni et al., 2011), we have verified the present microarray by qPCR on a selection of genes shown to be differentially expressed in this data set. These included neuronal genes that showed early differential expression at 2–4 months and astrocytic and immune genes that were differentially expressed at 8–18 months. qPCR was carried out both on the same tissue to check the consistency with the microarray data as well as on samples in which the mRNA was independently prepared from the brains of a different group of mice. In both cases, the data were almost entirely consistent (Figure S2).

Prior to use, the primers were tested for specificity by performing a test PCR reaction and resolving the samples on an agarose gel with ethidium bromide. The cDNA samples were tested in triplicate in a 20 μ l reaction volume in a 96-well plate format, containing 250 nM of each oligonucleotide primer and SYBR Green PCR Master Mix (BioRad). Negative control PCR reactions were also performed in parallel on total RNA that had not been processed with reverse transcriptase to test for the presence of genomic DNA in each sample with each primer pair. The cycling parameters were: 3 min at 95°C, followed by 40 cycles (95°C for 10 s, annealing at 58°C for 30 s, and extension at 72°C for 30 s), and then a melt-curve analysis was performed by holding the samples

at 95°C for 1 min and then increasing the temperature from 60°C to 95°C in 0.5°C increments every 5 s. The real-time PCR was performed in a CFX96 system with a C1000 thermal cycler (BioRad). We ensured that all qPCR reactions produced a single peak with the melt curve analysis. The results were expressed as $2^{-(\text{gene of interest mean Ct value} - \text{control gene mean Ct value})}$ for the qRT-PCR experiments. In order to increase the accuracy of gene expression levels for normalization, we used the mean of three internal control reference genes: *Rps28*, *Rps29*, and *Rpl4* (Vandesompele et al., 2002). Because the expression ratio of ideal control reference genes should be the same across all samples, we selected these reference genes among a set of 12 candidate reference genes that also included β-actin and *Rps18* in order to minimize the pairwise variation in gene expression across hippocampal tissues from different mice. The calculations were performed as described on the geNorm website (<http://medgen.ugent.be/~jvdesomp/genorm/>).

Data Analysis

All analyses were performed using R software and Partek Genomics Suite (Partek).

Raw expression data were log₂ transformed, and all samples were quantile normalized together. Individual probes were excluded from analyses if the detection p value was >0.05 in more than 50% of the samples in a given group at any age. Also, samples were excluded if <95% of the probes were detected. After these quality control steps, data were available for 113 hippocampus samples, 113 cortex samples, and 111 cerebellum samples representing 12,588 genes. Region, age, mouse strain and line, the interactions between these variables, as well as hybridization batch accounted for most of the data variance and were therefore included in the regression model. Unless otherwise specified, a conservative statistical threshold of FDR < 0.05 and minimum fold difference ≥ 1.5 between sample groups was used in all comparisons.

EASE (Subramanian et al., 2005) was used to identify enriched biological themes in gene lists using the DAVID database (<http://david.abcc.ncifcr.gov>). EASE uses a modified Fisher's exact test to determine whether the genes assigned to a GO, Kyoto Encyclopedia of Genes and Genomes grouping, and other experimentally derived genes that are overrepresented in gene categories relative to the population of genes investigated.

GO-ANOVA (Partek) was also used to find (1) differentially expressed functional groups of genes between the transgenic and control mice in the three brain regions and (2) changes in the pattern of gene expression within the functional group. In the first type of analysis, an ANOVA is performed at the gene level, but the result refers to the level of the functional group by averaging member gene results. In the second type of analysis, Z tests are used to compare the difference between each gene and the rest of the genes in the functional group, obtaining a disruption score that is the minimum p value from the Z test. Hippocampus, cortex, and cerebellum samples were analyzed separately after removing batch effect, and analyses were performed with their residuals.

For WGCNA, unsigned coexpression networks were built using the WGCNA package in R. Genes with variable expression patterns (coefficient of variation >5%) and normalized Log₂ expression values of at least 5 in any of the five transgenic groups, four ages, and three regions were selected for network analyses (Oldham et al., 2006). Therefore, 3,904 of the most-variable genes in a given tissue, age, disease state, and AD transgenic model were included in the analyses. WGCNA were performed on the selected genes as previously described (Horvath et al., 2006; Oldham et al., 2006; Zhang and Horvath, 2005). For each set of genes, a pairwise correlation matrix was computed and an adjacency matrix was calculated by raising the correlation matrix to a power. The power of 12 was chosen using the scale-free topology criterion and was used for each network using all AD transgenic and WT samples in each brain region.

For each pair of genes, a robust measure of network interconnectedness (topological overlap measure; Yip and Horvath, 2007) was calculated based on the adjacency matrix. The topological overlap-based dissimilarity was then used as input for average linkage hierarchical clustering: groups of genes based on the topological overlap of their connectivity. Branches of the resulting clustering tree were defined as gene modules (Langfelder et al., 2008). To cut the branches, we used hybrid dynamic tree cutting, a minimum module

size of 30 genes, and a minimum height for merging modules at 0.25. Each module was summarized by the first principal component of the scaled (standardized) module expression profiles. For each module, the module membership measure (aka module-eigengene-based connectivity kME) was defined as the correlation between gene-expression values and the module eigengene. Genes were assigned to a module if they had a high module membership (kME > 0.7). Each module was assigned a unique color identifier, and genes that did not fulfil these criteria for any of the modules were assigned to the gray module. For the cell-type-marker-enrichment analysis, we utilized the userListEnrichment function (Miller et al., 2011) in the WGCNA library. This function measures list enrichment between input lists of genes and files containing user-defined lists of genes using a hypergeometric test. We utilized the predefined brain lists corresponding to cell-type markers (astrocytes, neurons, oligodendrocytes, microglia, and macrophages) and genes found to be up- or downregulated with AD in any mouse or brain region.

ACCESSION NUMBERS

The NCBI GEO accession number for the data reported in this paper is GSE64398.

SUPPLEMENTAL INFORMATION

Supplemental Information includes three figures and five tables and can be found with this article online at <http://dx.doi.org/10.1016/j.celrep.2014.12.041>.

AUTHOR CONTRIBUTIONS

M.M. provided RNA extraction, microarray preparation, data analysis including network analysis, contribution to manuscript, and production of figures. D.A.S. and W.L. provided validation, qPCR, independent RNA samples, genotyping, and contribution to manuscript. D.M.C. provided organization of initial tissue for collection, tissue collection, and final production of figures. S.G. provided mouseac.org. M.Y., R.M.P., and S.S.A. provided immunohistochemistry preparation and analysis. M.A.N.S., R.D., and K.J.S. provided Aif1 staining and counts. M.P. provided contribution to microarray preparation and production of figures. M.F. and J.L. provided mouse supply, breeding and maintenance, tissue collection, and genotyping. J.C.R. provided GSK administration and comments on the manuscript. J.H. provided project planning, funding, comments on manuscript, and general organization. F.A.E. provided project planning, funding, writing manuscript, design of figures, and general organization.

ACKNOWLEDGMENTS

We would like to thank Rivka Steinberg for technical assistance. Funding was from a Medical Research Council UK Grant to F.A.E. (MR/J011851/1) and Alzheimer's Research UK. D.A.S. holds an Alzheimer's Research UK Fellowship. M.M. holds an Epilepsy Research UK Fellowship. M.P. holds a fellowship from National Atomic Energy Commission, Argentina. Thanks also for additional funding from IFRAD (French Alzheimer Association) through the IFRAD prize award to J.H. The transgenic mice for this study were supplied and/or used under a material transfer agreement with GSK. J.L., M.F., and J.C.R. were employed by GSK during this study.

Received: June 26, 2014

Revised: December 9, 2014

Accepted: December 18, 2014

Published: January 22, 2015

REFERENCES

- Barabási, A.L., and Oltvai, Z.N. (2004). Network biology: understanding the cell's functional organization. *Nat. Rev. Genet.* 5, 101–113.
- Dickey, C.A., Loring, J.F., Montgomery, J., Gordon, M.N., Eastman, P.S., and Morgan, D. (2003). Selectively reduced expression of synaptic

- plasticity-related genes in amyloid precursor protein + presenilin-1 transgenic mice. *J. Neurosci.* 23, 5219–5226.
- Driscoll, I., Troncoso, J.C., Rudow, G., Sojkova, J., Pletrikova, O., Zhou, Y., Kraut, M.A., Ferrucci, L., Mathis, C.A., Klunk, W.E., et al. (2012). Correspondence between *in vivo* [¹¹C]PiB-PET amyloid imaging and postmortem, region-matched assessment of plaques. *Acta Neuropathol.* 124, 823–831.
- Frank, S., Burbach, G.J., Bonin, M., Walter, M., Streit, W., Bechmann, I., and Deller, T. (2008). TREM2 is upregulated in amyloid plaque-associated microglia in aged APP23 transgenic mice. *Glia* 56, 1438–1447.
- Frautschy, S.A., Yang, F., Irrizarry, M., Hyman, B., Saido, T.C., Hsiao, K., and Cole, G.M. (1998). Microglial response to amyloid plaques in APPsw transgenic mice. *Am. J. Pathol.* 152, 307–317.
- Ghai, R., Waters, P., Roumenina, L.T., Gadjeva, M., Kojouharova, M.S., Reid, K.B., Sim, R.B., and Kishore, U. (2007). C1q and its growing family. *Immunobiology* 212, 253–266.
- Guerreiro, R.J., and Hardy, J. (2011). Alzheimer's disease genetics: lessons to improve disease modelling. *Biochem. Soc. Trans.* 39, 910–916.
- Guerreiro, R., Wojtas, A., Bras, J., Carrasquillo, M., Rogaeva, E., Majounie, E., Cruchaga, C., Sassi, C., Kauwe, J.S., Younkin, S., et al.; Alzheimer Genetic Analysis Group (2013). TREM2 variants in Alzheimer's disease. *N. Engl. J. Med.* 368, 117–127.
- Hartmann, D., De Strooper, B., and Saftig, P. (1999). Presenilin-1 deficiency leads to loss of Cajal-Retzius neurons and cortical dysplasia similar to human type 2 lissencephaly. *Curr. Biol.* 9, 719–727.
- Horvath, S., Zhang, B., Carlson, M., Lu, K.V., Zhu, S., Feliciano, R.M., Laurance, M.F., Zhao, W., Qi, S., Chen, Z., et al. (2006). Analysis of oncogenic signaling networks in glioblastoma identifies ASPM as a molecular target. *Proc. Natl. Acad. Sci. USA* 103, 17402–17407.
- Howlett, D.R., and Richardson, J.C. (2009). The pathology of APP transgenic mice: a model of Alzheimer's disease or simply overexpression of APP? *Histol. Histopathol.* 24, 83–100.
- Howlett, D.R., Bowler, K., Soden, P.E., Riddell, D., Davis, J.B., Richardson, J.C., Burbidge, S.A., Gonzalez, M.I., Irving, E.A., Lawman, A., et al. (2008). Abeta deposition and related pathology in an APP x PS1 transgenic mouse model of Alzheimer's disease. *Histol. Histopathol.* 23, 67–76.
- Hutton, M., Lendon, C.L., Rizzu, P., Baker, M., Froelich, S., Houlden, H., Pickering-Brown, S., Chakraverty, S., Isaacs, A., Grover, A., et al. (1998). Association of missense and 5'-splice-site mutations in tau with the inherited dementia FTDP-17. *Nature* 393, 702–705.
- Jonsson, T., Stefansson, H., Steinberg, S., Jónsdóttir, I., Jonsson, P.V., Snædal, J., Björnsson, S., Huttenlocher, J., Levey, A.I., Lah, J.J., et al. (2013). Variant of TREM2 associated with the risk of Alzheimer's disease. *N. Engl. J. Med.* 368, 107–116.
- Lagraoui, M., Latoche, J.R., Cartwright, N.G., Sukumar, G., Dalgaard, C.L., and Schaefer, B.C. (2012). Controlled cortical impact and craniotomy induce strikingly similar profiles of inflammatory gene expression, but with distinct kinetics. *Front Neurol* 3, 155.
- Langfelder, P., Zhang, B., and Horvath, S. (2008). Defining clusters from a hierarchical cluster tree: the Dynamic Tree Cut package for R. *Bioinformatics* 24, 719–720.
- Manook, A., Yousefi, B.H., Willuweit, A., Platzer, S., Reder, S., Voss, A., Huisman, M., Settles, M., Neff, F., Velden, J., et al. (2012). Small-animal PET imaging of amyloid-beta plaques with [¹¹C]PiB and its multi-modal validation in an APP/PS1 mouse model of Alzheimer's disease. *PLoS ONE* 7, e31310.
- Merino-Serrais, P., Benavides-Piccione, R., Blazquez-Llorca, L., Kastanauskaitė, A., Rábano, A., Avila, J., and DeFelipe, J. (2013). The influence of phospho- τ on dendritic spines of cortical pyramidal neurons in patients with Alzheimer's disease. *Brain* 136, 1913–1928.
- Miller, J.A., Cai, C., Langfelder, P., Geschwind, D.H., Kurian, S.M., Salomon, D.R., and Horvath, S. (2011). Strategies for aggregating gene expression data: the collapseRows R function. *BMC Bioinformatics* 12, 322.
- Mullan, M., Crawford, F., Axelman, K., Houlden, H., Lilius, L., Winblad, B., and Lannfelt, L. (1992). A pathogenic mutation for probable Alzheimer's disease in the APP gene at the N-terminus of beta-amyloid. *Nat. Genet.* 1, 345–347.
- Oldham, M.C., Horvath, S., and Geschwind, D.H. (2006). Conservation and evolution of gene coexpression networks in human and chimpanzee brains. *Proc. Natl. Acad. Sci. USA* 103, 17973–17978.
- Reddy, P.H., McWeney, S., Park, B.S., Manczak, M., Gutala, R.V., Partovi, D., Jung, Y., Yau, V., Searles, R., Mori, M., and Quinn, J. (2004). Gene expression profiles of transcripts in amyloid precursor protein transgenic mice: up-regulation of mitochondrial metabolism and apoptotic genes is an early cellular change in Alzheimer's disease. *Hum. Mol. Genet.* 13, 1225–1240.
- Richardson, J.C., Kendal, C.E., Anderson, R., Priest, F., Gower, E., Soden, P., Gray, R., Topps, S., Howlett, D.R., Lavender, D., et al. (2003). Ultrastructural and behavioural changes precede amyloid deposition in a transgenic model of Alzheimer's disease. *Neuroscience* 122, 213–228.
- Stein, T.D., and Johnson, J.A. (2002). Lack of neurodegeneration in transgenic mice overexpressing mutant amyloid precursor protein is associated with increased levels of transthyretin and the activation of cell survival pathways. *J. Neurosci.* 22, 7380–7388.
- Subramanian, A., Tamayo, P., Mootha, V.K., Mukherjee, S., Ebert, B.L., Gillette, M.A., Paulovich, A., Pomeroy, S.L., Golub, T.R., Lander, E.S., and Mesirov, J.P. (2005). Gene set enrichment analysis: a knowledge-based approach for interpreting genome-wide expression profiles. *Proc. Natl. Acad. Sci. USA* 102, 15545–15550.
- Thal, D.R., Del Tredici, K., and Braak, H. (2004). Neurodegeneration in normal brain aging and disease. *Sci. SAGE KE* 2004, pe26.
- Trabzuni, D., Ryten, M., Walker, R., Smith, C., Imran, S., Ramasamy, A., Weale, M.E., and Hardy, J. (2011). Quality control parameters on a large dataset of regionally dissected human control brains for whole genome expression studies. *J. Neurochem.* 119, 275–282.
- Vandesompele, J., De Preter, K., Pattyn, F., Poppe, B., Van Roy, N., De Paepe, A., and Speleman, F. (2002). Accurate normalization of real-time quantitative RT-PCR data by geometric averaging of multiple internal control genes. *Genome Biol.* 3, H0034.
- Varki, A., Geschwind, D.H., and Eichler, E.E. (2008). Explaining human uniqueness: genome interactions with environment, behaviour and culture. *Nat. Rev. Genet.* 9, 749–763.
- Wirz, K.T., Bossers, K., Stargardt, A., Kamphuis, W., Swaab, D.F., Hol, E.M., and Verhaagen, J. (2013). Cortical beta amyloid protein triggers an immune response, but no synaptic changes in the APPsw/PS1dE9 Alzheimer's disease mouse model. *Neurobiol. Aging* 34, 1328–1342.
- Wu, Z.L., Ciallella, J.R., Flood, D.G., O'Kane, T.M., Bozyczko-Coyne, D., and Savage, M.J. (2006). Comparative analysis of cortical gene expression in mouse models of Alzheimer's disease. *Neurobiol. Aging* 27, 377–386.
- Yip, A.M., and Horvath, S. (2007). Gene network interconnectedness and the generalized topological overlap measure. *BMC Bioinformatics* 8, 22.
- Zhang, B., and Horvath, S. (2005). A general framework for weighted gene co-expression network analysis. *Stat. Appl. Genet. Mol. Biol.* 4, e17.